Sinusoidal-Based Multiple Access Scheme for Visible Light Decentralized Asynchronous Systems

Siu-Wai Ho, Abdullah A Saed, Jean-Marie Gorce, Chung Shue Chen

Sinusoidal-Based Multiple Access Scheme for Visible Light Decentralized Asynchronous Systems

Siu-Wai Ho, *Senior Member, IEEE*, Abdullah A. Saed, Jean-Marie Gorce, *Senior Member, IEEE*, and Chung Shue Chen, *Senior Member, IEEE*

Abstract—In some visible light communication (VLC) systems, transmitters are light sources which support not only illumination but also information broadcast and positioning. Since transmit signals in these systems inevitably interfere with each other at the receiver side, extra devices may be added to synchronize the transmitters, but this impairs an appealing advantage in VLC systems that existing lighting infrastructure can be simply reused. This paper proposes a novel multiple access scheme to realize decentralized asynchronous VLC systems such that both the transmitters and receivers are asynchronous. For a system with N transmitters, two unique codewords of L chips are allocated to each transmitter where L is a prime number larger than $4N$. Those codewords are designed to help maintain a constant transmitted average power and enhance channel estimation, as well as conveying data. Our scheme enables the receiver to obtain one channel estimate and one data symbol per L chips. Simulation results show that the proposed scheme significantly outperforms other schemes in the literature in terms of bit error rate and system throughput.

Index Terms—Visible light communications, multiple access, channel estimation, decentralized asynchronous systems, indoor positioning.

I. INTRODUCTION

Future lighting systems can simultaneously provide communications and positioning service in addition to illumination [2–6]. These systems use light emitting diodes (LEDs) as transmitters and photo-detectors (PDs) as receivers so that intensity modulation and direct detection (IM/DD) are commonly used. This technology, Visible Light Communications (VLC), see e.g., [7], has recently gained a lot of attention as a promising future technology to overcome the scarcity of the radio frequency spectrum.

For information broadcast using VLC, many different schemes were proposed in the literature such as expurgated pulse position modulation [2], adaptive modulation based on power control [3] and Optical Code Division Multiple Access (OCDMA) [4]. All these schemes require a central unit and a backbone network to coordinate the LED transmission.

Some systems, however, do not need to support real time communications. For instance, a shopping mall or a museum can employ a visible light based positioning system [8–10]

Siu-Wai Ho is with Teletraffic Research Centre, University of Adelaide, Adelaide SA 5005, Australia, Email: siuwai.ho@adelaide.edu.au

Abdullah A. Saed is with University of South Australia, Adelaide SA 5001, Australia, Email: abdullah.saed@mymail.unisa.edu.au

Jean-Marie Gorce is with INRIA and University of Lyon, CITI, INSA Lyon, France, Email: jean-marie.gorce@inria.fr

Chung Shue Chen is with Bell Labs, Nokia Paris-Saclay Center, 91620 Nozay, France, Email: chung_shue.chen@nokia-bell-labs.com

A preliminary result of this work was presented in IEEE VTC'17 Spring [1].

in which each LED just needs to periodically broadcast its identity and constant message such as a local map. In such a system, if an asynchronous multiple access scheme that requires neither a central unit nor a backbone network for coordination is employed, the system's implementation and operational cost and complexity can be much reduced. Note also that transmitters (i.e., light sources) may be controlled by different switches and turned on/off at different time, implying that an asynchronous scheme is required. Therefore, we consider a decentralized asynchronous system (DAS) with properties:

1) no central unit is used,
2) no backbone communication network is needed, and
3) each transmitter independently encodes and starts to transmit its signals after an arbitrary time lag.

In a DAS system, direct communication link among the transmitters for time synchronization cannot be assumed. Besides, the channel gain between any transmitter-receiver pair is often random due to the receiver's random location and orientation during movement. Under these challenges, the receiver needs to estimate the channel gains and the messages broadcast by the LEDs.

A. Related Work

Several asynchronous multiple access schemes were proposed for VLC [10–16]. For the system in [10] with N transmitters, each transmitter is allocated a unique codeword of length 2^N and a receiver can completely eliminate multiple access interference (MAI) and decode the transmitted data. Each transmitter transmits only one symbol per codeword and hence the system throughput (equal to $\frac{N}{2^N}$) would degrade exponentially in N. The system throughput was improved to $1 - 2^{-N}$ in [11] by letting transmitter k send 2^{N-k} symbols over a codeword for $1 \leq k \leq N$. However, this system has a fairness issue due to the highly asymmetric rates among the transmitters.

An OCDMA scheme based on random optical codes was proposed in [12]. Random optical codes are simple to generate but they do not have ideal cross-correlation characteristics. Therefore, MAI would occur among the transmit signals and degrades the accuracy of channel gain estimation at the receiver. For positioning systems, since the estimated position is a function of the channel gain values, the positioning accuracy cannot be improved by using more received samples when MAI occurs. In [13], a preamble is incorporated prior to transmitting data to enable asynchronous communications.

For N transmitters, a code length greater than $10N$ is required for each user, while the preamble sequence length needs to be greater than or equal to $30N$ [14]. Thus, the system throughput is less than or equal to $\frac{1}{40}$ bits/chip, which is relatively low.

Cyclic Code-Shift Extension (CCSE) [15] was proposed to enhance the random optical codes of [13] in terms of cross-correlation property and system throughput. Due to MAI, the decoding of transmitted data still has errors even if the system is assumed to be noiseless. For example, codeword length needs to be greater than or equal to 150 in order to achieve bit error rate (BER) less than 10^{-3} in a system with 20 transmitters. In this case, the system throughput is upper bounded by $\frac{20}{150} = 0.133$ bits/chip. It should also be noted that the number of ones in a codeword is 3. Since the number of ones in the random optical codes is far less than the number of zeros, the average transmitted optical power is very small. Note that to satisfy the average optical power requirement for the illumination purpose in a VLC system in parallel to its communications or positioning purpose, a direct current (DC) offset may have to be added to the transmitted signals for the illumination but this would reduce the power consumption efficiency.

An optical Orthogonal Frequency Division Multiple Access (OFDMA) scheme with cyclic prefix or similar method is not suitable for DAS of VLC. A sub-carrier allocation based OFDMA scheme was proposed in [16] to mitigate the interference caused by the timing offset among LEDs. Cyclic prefix and filter bank based multi-carrier allocation were used. Their scheme however requires the timing offset to be so small that LED 1's signal vector $S(j)$ is within the duration of receiving LED 2's signal vector $S(i)$ and $S(i)$'s cyclic prefix, as shown in [16, Fig. 2(b)]. Since arbitrary timing offsets can occur in DAS, $S(j)$ may overlap with the cyclic prefixes of both $S(i)$ and $S(i+1)$.

Several problems have been identified in the above. Some existing schemes can completely eliminate MAI but they require long codeword lengths which would decrease the channel estimation rate and symbol transmission rate. Some schemes are relaxed to allow small MAI at the receiver which however would reduce the accuracy of a visible light based positioning system. In OFDMA scheme with cyclic prefix, transmitters are assumed to have small time lags (i.e., shorter than the length of cyclic prefix), but DAS cannot satisfy this assumption because the time lags in DAS are in general arbitrary. These problems can be solved by the scheme proposed in this paper.

B. Contributions

The main contributions of the paper are summarized below.
1) This paper proposes a novel multiple access scheme for VLC that has the properties:
   a) The scheme supports both information broadcast and channel estimation in a DAS, which are necessary for many existing visible light based positioning methods (see e.g., [5]), while avoiding MAI and minimizing the noise variance at the receiver side.
   b) Channel estimation is not affected by the randomness in transmit data so that the estimation of channel gain

can be done at a fixed rate independently.
   c) A flexible choice of data rate for VLC is supported.
2) Unbiased channel gain estimators are proposed. Their noise variance and computational complexity are analytically derived.
3) Simulation results are obtained and have shown that the proposed scheme significantly outperforms existing schemes in the literature in terms of the BER and system throughput when they are applied to a DAS.

This paper improves the preliminary result in [1] and has the following significant differences:
   i) This paper proposes a novel scheme, in which receivers can obtain an unbiased channel estimate per each codeword duration despite the transmit data randomness. Channel estimation rate is therefore much higher than the rate allowed in [1]. Simulation results in this paper illustrate a case that a received vector with length equal to 34 is sufficient for good channel estimation. In contrast, the scheme in [1] can achieve similar performance if the received vector length is 2311. Therefore, the scheme in this paper significantly reduces the length by 85%.
  ii) The work in this paper goes beyond the work in [1] by proposing a new estimator which has a lower computational complexity, without any performance degradation in comparison to the proposed estimator in [1].
 iii) New analytical results for our new proposed scheme are derived in this paper (see Section IV). The analytical results show the novelty and effectiveness of the proposed estimators.
  iv) Simulation results in Section V-D show that the new proposed scheme achieves more accurate channel estimation and smaller BER compared with the scheme in [1].

The rest of the paper is organized as follows. Section I-C describes some mathematical notations and operators used in this paper. Section II gives the system model and problem formulation. The proposed system including the transmitter design and the estimators used in the receiver are detailed in Section III. Section IV analyzes the system design and illustrates several important properties. Simulation results are shown in Section V before the discussion and conclusion are presented in Sections VI and VII, respectively.

C. Notation

For $\mu, m \in \mathbb{N}$, let $S(\mathbf{x}, \mu)$ be the cyclic shift of a row vector $\mathbf{x}$ to the left by μ elements and $\bar{S}(\mathbf{x}, \mu, m)$ is the truncated version of $S(\mathbf{x}, \mu)$ by keeping its first m elements. For example, $\bar{S}(\mathbf{x}, \mu, 0)$ is an empty vector. If $\mathbf{x} = (x_0, x_1, x_2)$, then $S(\mathbf{x}, 1) = (x_1, x_2, x_0)$ and $\bar{S}(\mathbf{x}, 1, 2) = (x_1, x_2)$. All the estimates of variables are denoted by the symbols of the original variables together with a hat. For example, the estimate of h is denoted by $\hat{h}$. For $\alpha, \beta \in \mathbb{N}$, define $\mathbf{0}_{\alpha \times \beta}$ and $\mathbf{1}_{\alpha \times \beta}$ as an $\alpha \times \beta$ matrix of zeros and an $\alpha \times \beta$ matrix of ones, respectively. For any matrix $\mathbf{M}$, let $\mathbf{M}^{\dagger} = \mathbf{M}^T (\mathbf{M}\mathbf{M}^T)^{-1}$ be the pseudo-inverse of $\mathbf{M}$ with $\mathbf{M}^T$ being the transpose of $\mathbf{M}$. The i-th element in a vector $\mathbf{c}$ is denoted by $\mathbf{c}[i]$ for $i \in \mathbb{N}$. This paper assumes that all matrices and vectors start from

TABLE I: Notation

Notation	Description
$S(\mathbf{x}, \mu)$	The cyclic shift of row vector $\mathbf{x}$ to the left by μ elements
$\bar{S}(\mathbf{x}, \mu, m)$	The truncation of $S(\mathbf{x}, \mu)$ by keeping its first m elements
$\mathbf{c}[i]$	The i-th element in a vector $\mathbf{c}$
$\hat{h}$	The estimate of variable h
$\mathbf{0}_{\alpha \times \beta}$	An $\alpha \times \beta$ matrix of zeros
$\mathbf{1}_{\alpha \times \beta}$	An $\alpha \times \beta$ matrix of ones
$\mathbf{M}^T$	The transpose of $\mathbf{M}$
$\mathbf{M}^\dagger$	The pseudo-inverse of $\mathbf{M}$, i.e., $\mathbf{M}^T(\mathbf{M}\mathbf{M}^T)^{-1}$
$\alpha \bmod \beta$	The remainder after dividing α by β
$\div$	The modular division under a finite field
$\lceil \cdot \rceil$	The ceiling function
$\lfloor \cdot \rfloor$	The floor function
$\lfloor \cdot \rceil$	Rounding to the nearest integer
$\angle(\cdot)$	The angle of a complex number in polar form

index zero. The ceiling and floor functions are denoted by $\lceil \cdot \rceil$ and $\lfloor \cdot \rfloor$, respectively. Let $\lfloor \cdot \rceil$ be rounding to the nearest integer. For $\alpha, \beta \in \mathbb{N}$, $\alpha \bmod \beta$ returns the remainder after dividing α by β. Define $\angle(\cdot)$ as the angle of a complex number in polar form within the range $[0, 2\pi)$. Let $\div$ be a modular division under a finite field.

II. SYSTEM MODEL AND PROBLEM FORMULATION

A. Channel Model

Consider a DAS with N transmitters and one receiver as shown in Fig. 1, which depicts the channel model for an arbitrary receiver in the system. Suppose each transmitter has one LED and transmits multiple data/message streams, while the receiver is a mobile device equipped with a PD. Define $b_i[k]$ as the k-th message sent by LED i. Let h_i be the channel gain between LED i and the receiver, which depends their distance, LED's irradiance angle, PD's incident angle, PD's responsivity and other factors [17, 18].

In a DAS, transmitters may start to transmit at different times. The time lag between the transmitter and receiver is explained here through Fig. 2. Let t and T be the time with respect to the receiver's clock and the LED i's clock, respectively. Suppose the receiver starts receiving signals at $t = 0$. Assume that LED i has started to transmit earlier by τ_i' units of time so that when $T = 0$, the receiver clock shows $t = -\tau_i'$. Therefore,

$$t = T - \tau_i'. \tag{1}$$

Define $x_i(t)$ as LED i's transmit signal that arrives at the receiver at time t. Assume that $x_i(0)$ was sent at $T = \tau_i \geq 0$ with respect to the transmitter clock as shown in Fig. 2. From (1), $x_i(0)$ was sent at $t = \tau_i - \tau_i'$ with respect to the receiver clock and hence, $\tau_i - \tau_i'$ can be seen as the propagation delay. Using $x_i(0)$ as a reference, it is ready to see that $x_i(t)$ was transmitted at $T = t + \tau_i$ with respect to the transmitter clock as shown in Fig. 2. Since LEDs may be switched on at different times, τ_i may be different for different i. Therefore, τ_i can be seen as the combined effect due to time lag and propagation delay. In the rest of this paper, τ_i' is not used and τ_i is assumed to be random.

Without loss of generality, the superposition of signals from all LEDs is captured together with the background light at the receiver [18]. Both the channel gains and the background light intensity are random over time but they are assumed to vary slightly in a short duration. Consider t within the channel coherence time such that h_i can be approximated as a constant. Then, the received signal can be represented by:

$$y(t) = \sum_{i=1}^{N} x_i(t) h_i + \Phi_0 + w(t), \tag{2}$$

where $\Phi_0 + w(t)$ is the additive noise. The DC-component in the noise, Φ_0, is mainly contributed by the background light intensity. The thermal noise and the fluctuation in the background light intensity around its mean are added together to become $w(t)$ which has zero mean. At the receiver, the signal $y(t)$ is sampled at a finite rate $\frac{1}{T_c}$, where T_c is the chip duration. Therefore, the discrete output contains one sample per chip. In this paper, we will focus on the case that the received power is dominated by the direct-line-of-sight (LoS) paths between the transmitters and the receiver.

B. Problem Formulation

Since the system is asynchronous, τ_i is unknown to the receiver. Furthermore, the receiver has no information about the channel gains h_i's and Φ_0 because the receiver can be at arbitrary location and with arbitrary orientation. Under these constraints, the important problem is how to design a communication scheme and also the transmitted waveform $x_i(t)$ such that for all i, the receiver can decode the broadcast message $b_i[k]$ from transmitter i and estimate h_i from the received signal $y(t)$.

III. PROPOSED MULTIPLE ACCESS SCHEME

In this section, we propose a sinusoidal-based multiple access (Sine-MA) scheme in a DAS. In contrast to the OFDMA scheme, our scheme requires codeword length to be prime, which is a critical assumption enabling our scheme to estimate the arbitrary time lags. Furthermore, our scheme requires no cyclic prefix but uses two codewords in a specific way such that MAI can be completely eliminated. Using two codewords incurs longer codeword length but has the benefits of improving channel estimation and BER because both codewords are used in the decoding phase and they provide redundancy to combat noise. The technical details are given below.

A. Transmitter Design

Definition 1. *Consider a prime $L > 4N$. For $1 \leq j \leq 2N$, let $\mathbf{c}_j$ be a codeword with L chips where the l-th chip of $\mathbf{c}_j$ is defined as:*

$$\mathbf{c}_j[l] = \cos\left(\frac{2\pi j l}{L}\right) + 1 \tag{3}$$

for $0 \leq l \leq L - 1$. Codewords $\mathbf{c}_{2i-1}$ and $\mathbf{c}_{2i}$ are assigned to LED i for $1 \leq i \leq N$.

Let b_i be an infinite-dimensional vector denoting the bit stream sent by LED i where $b_i[k] \in \{0, 1, \ldots, M-1\}$ is the
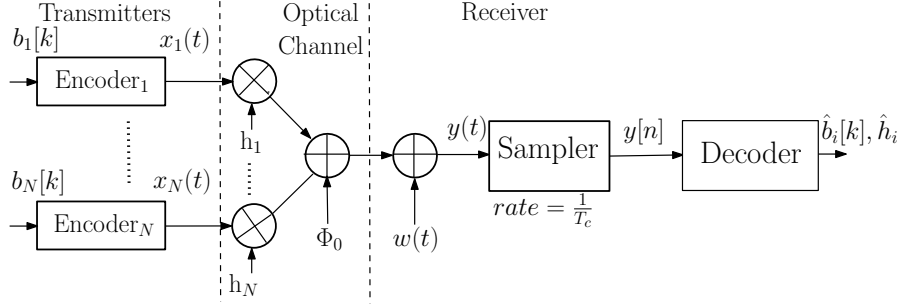
Fig. 1: A channel model of an asynchronous multiple access scheme in DAS for broadcasting N data streams by N transmitters.
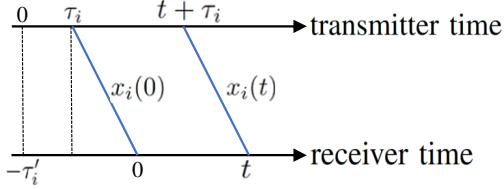

Fig. 2: Time lag and propagation delay experienced by a receiver. The slant blue lines indicate that signals are received after propagation delays.

k-th message symbol with integers $M \geq 2$ and $k \geq 0$. Each transmitter encodes its $b_i[k]$ independently. By letting

$$k_i = \left\lfloor \frac{t + \tau_i}{LT_c} \right\rfloor \quad and \quad l_i = \left\lfloor \frac{t + \tau_i}{T_c} \right\rfloor \qquad (4)$$

which depend on t, the waveform transmitted by LED i is given by

$$x_i(t) = \frac{\Phi_i}{M-1} \left(b_i[k_i]\mathbf{c}_{2i-1}[l_i] + (M - 1 - b_i[k_i])\mathbf{c}_{2i}[l_i] \right) \qquad (5)$$

where

$$\Phi_i = \frac{1}{LT_c} \int_{t=-\tau_i}^{LT_c - \tau_i} x_i(t)\, dt \qquad (6)$$

which is the average light intensity.

It is easy to see that $0 \leq \mathbf{c}_j[l] \leq 2$ and

$$\frac{1}{L} \sum_{l=0}^{L-1} \mathbf{c}_j[l] = 1 \qquad (7)$$

such that $x_i(t) \geq 0$.

B. Receiver Design

Suppose the receiver starts receiving signals at $t = 0$. Let

$$\eta_i = \left\lfloor \frac{\tau_i}{T_c} \right\rfloor \bmod L, \qquad (8)$$

where mod is the modulo operator. From l_i in (4) with $t = 0$, the first received chip is the η_i-th chip in the codewords. Therefore, η_i is seen to be the time lag for LED i experienced by the receiver. A summary of system parameters is shown in Fig. 3. The receiver first applies Algorithm 1 which requires the following definition.

Definition 2 (Estimation of time lag η_i). *Let*

$$\mathbf{B} = \begin{bmatrix} y(0) + y(LT_c) + \cdots + y((F-1)LT_c) \\ y(T_c) + y(T_c + LT_c) + \cdots + y(T_c + (F-1)LT_c) \\ \vdots \\ y((L-1)T_c) + y((2L-1)T_c) + \cdots + y((FL-1)T_c) \end{bmatrix} \qquad (9)$$

be a column vector with length L. Let $\tilde{\mathbf{B}}$ be the discrete Fourier transform (DFT) of $\mathbf{B}$. Denote the j-th element of $\tilde{\mathbf{B}}$ by $\hat{\mathbf{B}}[j]$. Define

$$\hat{\eta}_i = \left\lfloor \frac{(\angle(\tilde{\mathbf{B}}[2i-1]) + \angle(\tilde{\mathbf{B}}[2i]))L}{2\pi} \right\rceil \div (4i - 1), \qquad (10)$$

where $\div$ is a modular division under a finite field $\mathbb{F}(L)$.

The rationale of Algorithm 1 is explained here. Step 1 uses Definition 2 to estimate η_i from a received vector of length FL. Section IV-A will show that the probability of estimation error of η_i vanishes as $F \to \infty$. The probability of estimation error decays exponentially fast and is less than 10^{-4} for $F > 20$ in the simulations results in Section IV-A. Other steps in Algorithm 1 process a received vector of νL symbols to prepare the output variables including ξ, $\mathbf{C}$ and $\mathbf{Y}$ which will be used for channel gain and data estimation later on. Steps 3 to 10 search for ξ such that $\mathbf{C}$ is pseudo-invertible, i.e., $\mathbf{C}\mathbf{C}^T$ is invertible. In all the simulation results in Section V, Algorithm 1 can always find a pseudo-invertible $\mathbf{C}$ without reaching the error case $\xi = L$ in Step 9.

Remarks:
1) Here, F and ν are system parameters to be determined. For different values of F and ν, the receiver complexity and simulation result will be shown in Section IV-E and Section V-B, respectively.
2) $\mathbf{C}$ depends on ξ because from (14), it is composed of $\tilde{\mathbf{C}}_j$ which is related to $\mathbf{Y}$ through (13).
3) In Step 5, if $\hat{\eta}_i = 0$, the last row in (12) is a zero row. In such case, the last row in $\tilde{\mathbf{C}}_j$ and the last element in $\mathbf{V}_i$ are removed, thus $\tilde{\mathbf{C}}_j$ and $\mathbf{V}_i$ become a $\nu \times (\nu L)$ matrix and a row vector with length ν, respectively.
4) The transmit waveform in (5) may not have ideal rising/falling edges in practice. If the edges are received at $t = jT_c$ for $j \in \mathbb{N}$, the decoded message may contain a lot of errors. This paper assumes that the edges are
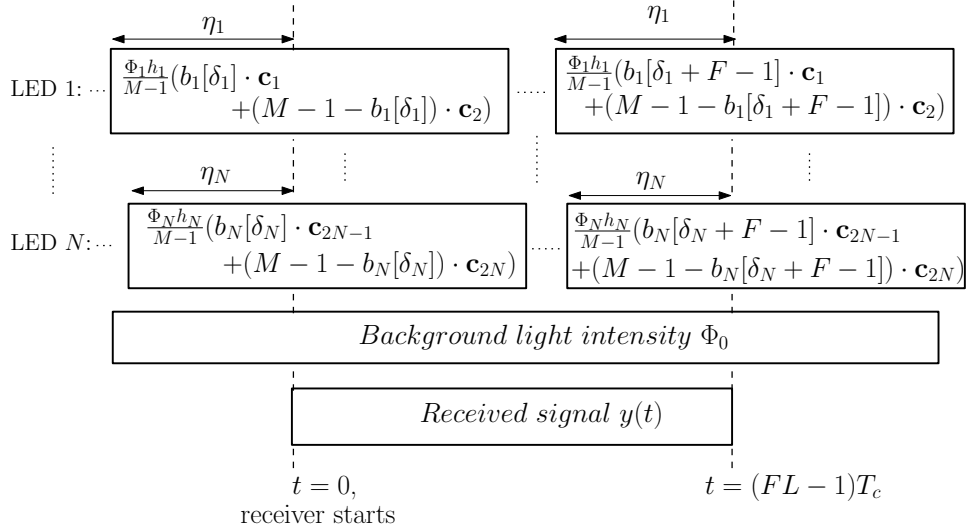
Fig. 3: Time lags among transmitters when a block of signals is received for time lag estimation.

sufficiently narrow and the receiver can always find a delay δ such that $y(jT_c + \delta)$ does not overlap with any edge transmitted from the LEDs.

C. Two Channel Estimators

Let $\Gamma(k)$ be the number of rows in $\tilde{\mathbf{C}}_k$ and let $\gamma = \Gamma(1)$, i.e., the number of rows in $\tilde{\mathbf{C}}_1$. Note that $\Gamma(k)$ varies over k because it depends on Step 5 in Algorithm 1. If we consider the estimation of h_i for an arbitrary i, the analysis would consist of cumbersome notations with the summations of $\Gamma(k)$, such as $\sum_{k:k<i} \Gamma(k)$ and $\sum_{k:k>i+1} \Gamma(k)$. To simplify the notations and without loss of generality, assume that the receiver wants to estimate h_1 and decode $b_1[\cdot]$ sent from LED 1 in the following. If the receiver is interested in LED i instead, it can proceed by swapping $(\tilde{\mathbf{C}}_1, \tilde{\mathbf{C}}_2)$ and $(\tilde{\mathbf{C}}_{2i-1}, \tilde{\mathbf{C}}_{2i})$ in (14).

The minimal noise variance estimator (MNE) in Algorithm 2 can be applied to estimate channel gain. The reason behind the definition of $\mathbf{A}$ is that from [19, P. 304], $\boldsymbol{\beta}^*$ in (19) is the solution of a linear optimization problem

$$\underset{\boldsymbol{\beta}}{\text{minimize}} \quad |\boldsymbol{\beta}|^2 \tag{23}$$

$$\text{subject to} \quad \mathbf{A}\boldsymbol{\beta} = \mathbf{e}. \tag{24}$$

Due to (15) and (16), the interference from ambient light and other LEDs are eliminated. The randomness in the transmit messages does not affect the estimated channel gain due to (17). The presence of (18) avoids the useless solution $\boldsymbol{\beta} = \mathbf{0}_{(\nu L) \times 1}$. These properties will be formally justified when the MNE is shown to be unbiased in the proof of Theorem 2. Since the noise variance is shown to be proportional to $|\boldsymbol{\beta}|^2$ in Section IV-B, the solution $\boldsymbol{\beta}^*$ achieves the minimal noise variance subject to the constraints from (15)–(18).

The Pseudo-Inverse Estimator (PIE) from Algorithm 3 is an alternative estimator obtained from the maximal ratio combining of the set of estimators $(d_j + d_{j+\gamma})$. As shown in Section IV, it also satisfies the constraints from (15)–(18) and a smaller complexity compared with MNE.

D. Estimation of Channel Gains and Data

Finally, we define a decoder that estimates h_1 and produces a stream of estimated symbols $\hat{b}_1$ at the same rate of $\frac{1}{T_c L}$. In Algorithm 4, $b_1[k]$ and $M - 1 - b_1[k]$ can be estimated by $\boldsymbol{\alpha}'$ and $\boldsymbol{\alpha}''$, respectively. These two estimates are combined to estimate $b_1[k]$ in (26).

Remarks:
1) The choice of $\boldsymbol{\beta}$ in Step 1 depends on the desired receiver complexity. The calculations for obtaining $\boldsymbol{\alpha}$ and $\boldsymbol{\beta}$ need to be done only once in Steps 1–2. The same $\boldsymbol{\alpha}$ and $\boldsymbol{\beta}$ are used until η_i is changed for some i that may happen when transmitter i is switched off and then on later.
2) The loop from Steps 3–6 involves only simple multiplications using $\boldsymbol{\alpha}$ and $\boldsymbol{\beta}$.
3) A set of consecutive symbols $b_1[k], b_1[k+1], \ldots$ is estimated from (26). Although the receiver does not know k, the transmitter can add a header or a preamble such that the receiver can determine the beginning of a message.
4) To construct $\mathbf{Y}$ in (11), the receiver needs to wait for a duration of $\nu L T_C$ which is the latency of the system. The latency for some practical cases will be evaluated in Section 1.

IV. ANALYSIS OF SYSTEM DESIGN

The Sine-MA scheme defined in Section III is analyzed in this section. The estimation of time lag is shown to be reliable for sufficiently large F. The estimators for channel gains and data are analyzed and their complexity is shown. Finally, channel estimation rate and symbol rate are discussed.

A. Estimation of Time Lag

The following theorem illustrates that Definition 2 provides a reliable estimation of η_i as long as F is sufficiently large.

Algorithm 1 Construction of coding matrix $\mathbf{C}$ and shift ξ

1: Obtain $\hat{\eta}_i$ from Definition 2.
2: Set $\xi = 0$.
3: Let

$$\mathbf{Y} = [y(\xi T_C) \quad y((\xi+1)T_C) \quad \cdots \quad y((\xi+\nu L-1)T_C)]. \tag{11}$$

4: For $1 \leq j \leq 2N$, let $i = \lceil \frac{j}{2} \rceil$ and then construct a $(\nu+1) \times (\nu L)$ matrix:

$$\tilde{\mathbf{C}}_j = \begin{bmatrix} \bar{S}(\mathbf{c}_j, \hat{\eta}_i, L-\hat{\eta}_i) & 0 & 0\cdots & 0 & 0 \\ 0 & \mathbf{c}_j & 0\cdots & 0 & 0 \\ \vdots & & \ddots & & \vdots \\ 0 & 0 & 0 & \mathbf{c}_j & 0 \\ 0 & 0 & 0 & 0 & \bar{S}(\mathbf{c}_j, 0, \hat{\eta}_i) \end{bmatrix}. \tag{12}$$

According to (2) and (5), $\mathbf{Y}$ can be rewritten as:

$$\mathbf{Y} = \sum_{i=1}^{N} \frac{\Phi_i h_i}{M-1}(\mathbf{V}_i\tilde{\mathbf{C}}_{2i-1} + (M-1-\mathbf{V}_i)\tilde{\mathbf{C}}_{2i}) \\ + \Phi_0 \mathbf{1}_{1\times\nu L} + \mathbf{w}, \tag{13}$$

where $\mathbf{V}_i = [b_i[k_i] \; b_i[k_i+1] \; \cdots \; b_i[k_i+\nu]]$ with k_i given in (4) at $t = \xi T_C$ and $\mathbf{w}$ is a row vector of length νL (i.e., the sampling of $w(t)$).
5: If $\hat{\eta}_i = 0$, the last row in (12) is a zero row. In this case, the last row in $\tilde{\mathbf{C}}_j$ and the last element in $\mathbf{V}_i$ are removed.
6: Let

$$\mathbf{C} = [\tilde{\mathbf{C}}_1^T \quad \tilde{\mathbf{C}}_2^T \quad \cdots \quad \tilde{\mathbf{C}}_{2N}^T \quad \mathbf{1}_{\nu L \times 1}]^T. \tag{14}$$

7: Go to Step 11 if $\mathbf{C}\mathbf{C}^T$ is invertible.
8: Set $\xi = \xi + 1$ and replace $\hat{\eta}_i$ by $((\hat{\eta}_i + 1) \mod L)$.
9: If $\xi = L$, declare errors and terminate the algorithm.
10: Go to Step 3 to update $\mathbf{Y}$ and $\tilde{\mathbf{C}}_j$ according to the new values of ξ and $\hat{\eta}_i$.
11: Output ξ, $\mathbf{C}$, $\mathbf{C}^\dagger$ and $\mathbf{Y}$ and terminate.

Theorem 1. *Suppose $\hat{\eta}_i$ is obtained from (10). Assume that the distribution of $b_i[k]$ is uniform for all i, k. For F sufficiently large and any $\varepsilon > 0$,*

$$\Pr\{\hat{\eta}_i = \eta_i, \; \forall i\} > 1 - \varepsilon. \tag{27}$$

Proof. By substituting (5) in (2),

$$y(t) \\ = \sum_{i=1}^{N} \frac{\Phi_i h_i}{M-1}(b_i[k_i]\mathbf{c}_{2i-1}[l_i] + (M-1-b_i[k_i])\mathbf{c}_{2i}[l_i]) \\ + \Phi_0 + w(t), \tag{28}$$

where k_i and l_i on the right side depends on t due to (4). By

---

Algorithm 2 Minimal Noise variance Estimator (MNE)

1: Obtain $\mathbf{Y}$ and $\mathbf{C}$ from Algorithm 1.
2: For a column vector $\boldsymbol{\beta}$ with νL real numbers, rewrite the linear equations

$$\mathbf{1}_{1\times\nu L} \cdot \boldsymbol{\beta} = 0, \tag{15}$$
$$\tilde{\mathbf{C}}_k \cdot \boldsymbol{\beta} = \mathbf{0}_{\Gamma(k)\times 1}, \qquad \text{for } k > 2 \tag{16}$$
$$(\tilde{\mathbf{C}}_1 - \tilde{\mathbf{C}}_2) \cdot \boldsymbol{\beta} = \mathbf{0}_{\gamma\times 1}, \tag{17}$$
$$\mathbf{1}_{1\times\gamma} \cdot \tilde{\mathbf{C}}_2 \cdot \boldsymbol{\beta} = 1, \tag{18}$$

in the form $\mathbf{A}\boldsymbol{\beta} = \mathbf{e}$ where $\mathbf{A}$ is a $\omega \times (\nu L)$ matrix and $\mathbf{e}$ is a column vector having $\omega - 1$ zeros together with the last element equal to one where $\omega = 2 + \sum_{k=2}^{2N} \Gamma(k)$.
3: Let

$$\boldsymbol{\beta}^* = \mathbf{A}^\dagger \mathbf{e}. \tag{19}$$

4: The MNE estimate of the channel gain is given by:

$$\hat{h}_1 = \frac{\mathbf{Y}\boldsymbol{\beta}^*}{\Phi_1}. \tag{20}$$

Algorithm 3 Pseudo-Inverse Estimator (PIE)

1: Obtain $\mathbf{C}$, $\mathbf{C}^\dagger$ and $\mathbf{Y}$ from Algorithm 1.
2: For $0 \leq j < \gamma$, let $\mathbf{d}_j$ be the j-th column in $\mathbf{C}^\dagger$.
3: Define the PIE as:

$$\boldsymbol{\beta}' = \sum_{j=0}^{\gamma-1} \left(\sum_{i=0}^{\gamma-1} \frac{|\mathbf{d}_j + \mathbf{d}_{j+\gamma}|^2}{|\mathbf{d}_i + \mathbf{d}_{i+\gamma}|^2} \right)^{-1} (\mathbf{d}_j + \mathbf{d}_{j+\gamma}). \tag{21}$$

4: The PIE estimate of the channel gain is given by:

$$\hat{h}_1 = \frac{\mathbf{Y}\boldsymbol{\beta}'}{\Phi_1}. \tag{22}$$

Algorithm 4 Channel Estimator and Data Decoder

1: Obtain ξ, $\mathbf{C}$, $\mathbf{C}^\dagger$ and $\mathbf{Y}$ from Algorithm 1.
2: Let $\boldsymbol{\beta}$ be either MNE $\boldsymbol{\beta}^*$ or PIE $\boldsymbol{\beta}'$ from Algorithms 2 or 3, respectively.
3: Let $\boldsymbol{\alpha} = \boldsymbol{\alpha}' - \boldsymbol{\alpha}''$ where $\boldsymbol{\alpha}'$ and $\boldsymbol{\alpha}''$ are the $\lfloor \frac{\gamma}{2} \rfloor$-th and $(\lfloor \frac{\gamma}{2} \rfloor + \gamma)$-th columns in $\mathbf{C}^\dagger$, respectively.
4: The channel gain is estimated by:

$$\hat{h}_1 = \frac{\mathbf{Y}\boldsymbol{\beta}}{\Phi_1}. \tag{25}$$

5: The message symbol is estimated by

$$\hat{b}_1 = \frac{M-1}{2\Phi_1\hat{h}_1}\mathbf{Y}\boldsymbol{\alpha} + \frac{M-1}{2}. \tag{26}$$

6: Update ξ by $\xi + L$ and update $\mathbf{Y}$ according to (11).
7: Go back Step 4.

substituting $t = nT_c$,

$$y(nT_c)$$
$$= \sum_{i=1}^{N} \frac{\Phi_i h_i}{M-1} \left(b_i[\tilde{k}_{n,i}] \mathbf{c}_{2i-1}[\tilde{l}_{n,i}] + (M-1-b_i[\tilde{k}_{n,i}]) \mathbf{c}_{2i}[\tilde{l}_{n,i}] \right)$$
$$+ \Phi_0 + w(nT_c), \tag{29}$$

where $\tilde{k}_{n,i} = \left\lfloor \frac{nT_c + \tau_i}{LT_c} \right\rfloor$ and $\tilde{l}_{n,i} = n + \left\lfloor \frac{\tau_i}{T_c} \right\rfloor = n + \eta_i$ from (4). So, the expected value of the $(j+1)$-th element in $\mathbf{B}$ is expressible as:

$$\sum_{f=0}^{F-1} \mathbb{E}\left[y(jT_c + fLT_c) \right]$$
$$= \sum_{f=0}^{F-1} \left(\sum_{i=1}^{N} \frac{\Phi_i h_i}{M-1} \left(\mathbb{E}[b_i[\tilde{k}_{n,i}]] \mathbf{c}_{2i-1}[\tilde{l}_{n,i}] + \right. \right.$$
$$\left. \left. (M-1-\mathbb{E}[b_i[\tilde{k}_{n,i}]]) \mathbf{c}_{2i}[\tilde{l}_{n,i}] \right) + \Phi_0 \right), \tag{30}$$

which is obtained from (29) with $n = j + fL$ and $\mathbb{E}[w(nT_c)] = 0$. Note that

$$\mathbb{E}[b_i[\tilde{k}_{n,i}]] = \frac{M-1}{2} \tag{31}$$

as $b_i[\cdot]$ is uniformly distributed in $\{0, 1, \ldots, M-1\}$. Furthermore,

$$\mathbf{c}_{2i}[\tilde{l}_{n,i}] = \mathbf{c}_{2i}[n + \eta_i] = \mathbf{c}_{2i}[j + fL + \eta_i] = \mathbf{c}_{2i}[j + \eta_i], \tag{32}$$

where the last equality follows from (3). Since the right sides of both (31) and (32) are independent of f, (30) becomes:

$$\sum_{f=0}^{F-1} \mathbb{E}\left[y(jT_c + fLT_c) \right]$$
$$= \sum_{i=1}^{N} \frac{\Phi_i h_i}{M-1} \left(\frac{F(M-1)}{2} \left(\mathbf{c}_{2i-1}[j + \eta_i] - \mathbf{c}_{2i}[j + \eta_i] \right) \right.$$
$$\left. + F(M-1) \mathbf{c}_{2i}[j + \eta_i] \right) + F\Phi_0$$
$$= F \sum_{i=1}^{N} \frac{\Phi_i h_i}{2} \left(\mathbf{c}_{2i-1}[j + \eta_i] + \mathbf{c}_{2i}[j + \eta_i] \right) + F\Phi_0. \tag{33}$$

Therefore,

$$\lim_{F \to \infty} \frac{\mathbb{E}[\mathbf{B}]}{F}$$
$$= \begin{bmatrix} \sum_{i=1}^{N} \frac{\Phi_i h_i}{2} \left(\mathbf{c}_{2i-1}[\eta_i] + \mathbf{c}_{2i}[\eta_i] \right) + \Phi_0 \\ \vdots \\ \sum_{i=1}^{N} \frac{\Phi_i h_i}{2} \left(\mathbf{c}_{2i-1}[L-1+\eta_i] + \mathbf{c}_{2i}[L-1+\eta_i] \right) + \Phi_0 \end{bmatrix}$$
$$= \sum_{i=1}^{N} \frac{h_i \Phi_i}{2} \cdot \left(S(\mathbf{c}_{2i-1}^T, \eta_i) + S(\mathbf{c}_{2i}^T, \eta_i) \right) + \Phi_0$$
$$= \sum_{i=1}^{N} \frac{h_i \Phi_i}{2} \cdot \left(S(\mathbf{c}_{2i-1}^T - 1, \eta_i) + S(\mathbf{c}_{2i}^T - 1, \eta_i) \right)$$
$$+ \sum_{i=1}^{N} h_i \Phi_i + \Phi_0, \tag{34}$$

where the right side of (34) is equivalent to the superposition of a set of orthogonal cosine waves

$$\frac{h_i \Phi_i}{2} \cos \left(2\pi \frac{j}{L} t + \frac{2\pi j \eta_i}{L} \right) \tag{35}$$

with $i = \lfloor \frac{j}{2} \rfloor$ for $1 \le j \le 2N$ being sampled at $t = 0, 1, \ldots, L-1$ in the presence of a constant $\Phi_0 + \sum_i h_i \Phi_i$. Since $L > 4N$ in Definition 1, the frequency of (35) is upper bounded by $\frac{2N}{L} < \frac{1}{2}$ and hence, the sampling rate equal to 1 is over the Nyquist sampling rate. Therefore, the angle of the j-th element in $\tilde{\mathbf{B}}$, i.e., the discrete Fourier transform of $\mathbf{B}$, will tend to the phase shift in (35) as $F \to \infty$. However, the angle is upper bounded by 2π so that

$$\lim_{F \to \infty} \mathbb{E}[\tilde{\mathbf{B}}[j]] = \frac{2\pi j \eta_i}{L} - 2\pi\psi_j, \tag{36}$$

where ψ_j is an integer such that the right side of (36) is less than 2π. Let $\zeta = 1 \div (4i-1)$ in $\mathbb{F}(L)$ so that $\zeta(4i-1) \bmod L = 1$. From (10) and (36),

$$\lim_{F \to \infty} \mathbb{E}[\hat{\eta}_i]$$
$$= \left(\left\lfloor \frac{\left(\frac{2\pi(2i-1)\eta_i}{L} - 2\pi\psi_{2i-1} + \frac{2\pi 2 i \eta_i}{L} - 2\pi\psi_{2i} \right) L}{2\pi} \right\rfloor \right.$$
$$\left. \div (4i-1) \right) \bmod L$$
$$= \left(((4i-1)\eta_i + (\psi_{2i-1} + \psi_{2i})L) \div (4i-1) \right) \bmod L$$
$$= \left(\zeta(4i-1)\eta_i + \zeta(\psi_{2i-1} + \psi_{2i})L \right) \bmod L$$
$$= \eta_i. \tag{37}$$

In other words, for any $\varepsilon' > 0$ and F sufficiently large,

$$\mathbb{E}[|\hat{\eta}_i - \eta_i|] < \varepsilon'. \tag{38}$$

Together with Markov's inequality, the theorem is proved. $\square$

The assumption of $b_i[k]$ being uniformly distributed in Theorem 1 can be achieved in practice if data are compressed before transmission (see the discussion below Lemma 13.3.1 in [20]). Alternatively, algorithms such as [21] can be applied to regulate the probability distribution. Theorem 1 suggests to use a large F. Since $\mathbf{B}$ in (9) is a column vector with length L, the complexity of the most computational demanding task in Definition 2, i.e., the discrete Fourier transform, is independent of F. Comparing with the complexity of evaluating [1, Eqn. (8)] which grows in K (which is equivalent to F in this paper), Definition 2 is better for a large F.

B. Estimation of Channel Gain

The estimated channel gain in (25) is obtained from applying either MNE or PIE. In the following, both are them are proved to be unbiased and zero-forcing (ZF), i.e., without MAI. The proofs require the following two lemmas. Let $\mathbf{e}_\ell$ be a column vector with γ elements equal to zeros except the ℓ-th element equal to 1.

Lemma 1. Both $\tilde{\mathbf{C}}_1$ and $\tilde{\mathbf{C}}_2$ have γ rows.

Proof. From Steps 4 and 5 in Algorithm 1, both $\tilde{\mathbf{C}}_1$ and $\tilde{\mathbf{C}}_2$ have $\nu+1$ rows if $\hat{\eta}_i > 0$. They have ν rows if $\hat{\eta}_i = 0$. Together

with the assumption at the beginning of Section III-C that γ is the number of rows in $\tilde{\mathbf{C}}_1$, the lemma is proved. $\square$

Lemma 2. *Consider* $1 \leq \ell \leq 2\gamma$ *and* $1 \leq k \leq 2N$. *If* $\mathbf{d}_\ell$ *is the* ℓ-*th column in* $\mathbf{C}^\dagger$,

$$\mathbf{1}_{1 \times \nu L} \cdot \mathbf{d}_\ell = 0 \tag{39}$$

and

$$\tilde{\mathbf{C}}_k \mathbf{d}_\ell = \begin{cases} \mathbf{e}_\ell & \text{if } \ell \leq \gamma \text{ and } k = 1 \\ \mathbf{e}_{\ell-\gamma} & \text{if } \gamma < \ell \text{ and } k = 2 \\ \mathbf{0}_{\Gamma(k) \times 1} & \text{otherwise.} \end{cases} \tag{40}$$

Proof. We first verify (39). Note that $\mathbf{C}\mathbf{C}^\dagger$ is an identity matrix $\mathbf{I}$. Since $\mathbf{1}_{1 \times \nu L}$ is the last row in $\mathbf{C}$ from (14), $\mathbf{1}_{1 \times \nu L}\mathbf{d}_\ell$ is the last element in the ℓ-th column in $\mathbf{I}$. Since $\ell \leq 2\gamma$, $\mathbf{1}_{1 \times \nu L}\mathbf{d}_\ell = 0$.

From (14) and Lemma 1, $\tilde{\mathbf{C}}_1$ locates at the top γ rows in $\mathbf{C}$, $\tilde{\mathbf{C}}_2$ locates from the $(\gamma+1)$-th to the (2γ)-th row in $\mathbf{C}$ and $\tilde{\mathbf{C}}_k$ for $k > 2$ locates in some rows below the (2γ)-th row in $\mathbf{C}$. Therefore, $\tilde{\mathbf{C}}_1 \mathbf{d}_\ell$ is the vector of the first γ elements in the ℓ-th column in $\mathbf{I}$, and hence $\tilde{\mathbf{C}}_1 \mathbf{d}_\ell$ is a column vector of zeros except its ℓ-th element equal to 1 for $1 \leq \ell \leq \gamma$. Similarly, $\tilde{\mathbf{C}}_2 \mathbf{d}_\ell$ is the vector of the $(\gamma+1)$-th to the (2γ)-th elements in the ℓ-th column in $\mathbf{I}$, $\tilde{\mathbf{C}}_2 \mathbf{d}_\ell$ is a column vector of zeros except its $(\ell - \gamma)$-th element equal to 1 for $\gamma + 1 \leq \ell \leq 2\gamma$. For $k > 2$, $\tilde{\mathbf{C}}_k \mathbf{d}_\ell$ is the vector of the γ elements located below the (2γ)-th row in the ℓ-th column in $\mathbf{I}$. Since $\ell \leq 2\gamma$, $\tilde{\mathbf{C}}_k \mathbf{d}_\ell$ is a column vector of zeros. Therefore, (39) is verified. $\square$

Theorem 2. *The MNE in Algorithm 2 is an unbiased ZF estimator and its output in* (20) *is equal to*

$$h_1 + \frac{\mathbf{w}\boldsymbol{\beta}^*}{\Phi_1}. \tag{41}$$

Proof. From (13) and (20),

$$\frac{\mathbf{Y}\boldsymbol{\beta}^*}{\Phi_1}$$

$$= \sum_{i=1}^{N} \left(\frac{\Phi_i h_i}{M-1} \mathbf{V}_i (\tilde{\mathbf{C}}_{2i-1} - \tilde{\mathbf{C}}_{2i}) + \Phi_i h_i \mathbf{1}_{1 \times \Gamma(2i)} \cdot \tilde{\mathbf{C}}_{2i} \right) \frac{\boldsymbol{\beta}^*}{\Phi_1}$$
$$+ \frac{\Phi_0 \mathbf{1}_{1 \times \nu L} \cdot \boldsymbol{\beta}^*}{\Phi_1} + \frac{\mathbf{w}\boldsymbol{\beta}^*}{\Phi_1} \tag{42}$$

$$= \sum_{i=1}^{N} \left(\frac{\Phi_i h_i}{M-1} \mathbf{V}_i (\tilde{\mathbf{C}}_{2i-1} - \tilde{\mathbf{C}}_{2i}) + \Phi_i h_i \mathbf{1}_{1 \times \Gamma(2i)} \cdot \tilde{\mathbf{C}}_{2i} \right) \frac{\boldsymbol{\beta}^*}{\Phi_1}$$
$$+ \frac{\mathbf{w}\boldsymbol{\beta}^*}{\Phi_1} \tag{43}$$

$$= \left(\frac{\Phi_1 h_1}{M-1} V_1 (\tilde{\mathbf{C}}_1 - \tilde{\mathbf{C}}_2) + \Phi_1 h_1 \mathbf{1}_{1 \times \gamma} \cdot \tilde{\mathbf{C}}_2 \right) \frac{\boldsymbol{\beta}^*}{\Phi_1} + \frac{\mathbf{w}\boldsymbol{\beta}^*}{\Phi_1} \tag{44}$$

$$= h_1 \mathbf{1}_{1 \times \gamma} \cdot \tilde{\mathbf{C}}_2 \boldsymbol{\beta}^* + \frac{\mathbf{w}\boldsymbol{\beta}^*}{\Phi_1} \tag{45}$$

$$= h_1 + \frac{\mathbf{w}\boldsymbol{\beta}^*}{\Phi_1}, \tag{46}$$

where (43) is obtained from (15). Due to (16) and Lemma 1, (44) is obtained. The vector of message symbols $\mathbf{V}_1$ disappears in (45) due to (17). Finally, (46) follows from (18). MNE

is therefore a ZF estimator and unbiased due to $\mathbf{w}$ has zero mean.

$\square$

Theorem 3. *The PIE in Algorithm 3 is an unbiased ZF estimator and the maximum ratio combining of the set of estimators* $(\mathbf{d}_j + \mathbf{d}_{j+\gamma})$. *Its output in* (22) *is equal to*

$$h_1 + \frac{\mathbf{w}\boldsymbol{\beta}'}{\Phi_1}. \tag{47}$$

Proof. Let

$$\tilde{\mathbf{V}}_i = \frac{\Phi_i h_i}{M-1} \cdot [\mathbf{V}_i \quad (M-1-\mathbf{V}_i)] \tag{48}$$

and

$$\mathbf{V} = [\tilde{\mathbf{V}}_1 \quad \tilde{\mathbf{V}}_2 \quad \cdots \quad \tilde{\mathbf{V}}_N \quad \Phi_0]. \tag{49}$$

According to Step 5 in Algorithm 1, the number of elements in $\mathbf{V}_i$ is the same as the number of rows in $\tilde{\mathbf{C}}_i$, i.e., $\Gamma(i)$. Therefore, $\mathbf{V}_1$ and $\tilde{\mathbf{V}}_1$ have γ and 2γ elements, respectively. Then

$$\tilde{\mathbf{V}}_1 \cdot [\mathbf{e}_j^T \quad \mathbf{e}_j^T]^T \tag{50}$$

$$= \frac{\Phi_1 h_1}{M-1} \cdot [\mathbf{V}_1 \quad (M-1-\mathbf{V}_1)] \cdot [\mathbf{e}_j^T \quad \mathbf{e}_j^T]^T \tag{51}$$

$$= \frac{\Phi_1 h_1}{M-1} \cdot [\mathbf{V}_1 \cdot \mathbf{e}_j + (M-1-\mathbf{V}_1) \cdot \mathbf{e}_j] \tag{52}$$

$$= \Phi_1 h_1. \tag{53}$$

From (13), $\mathbf{Y}$ can be rewritten as $\mathbf{Y} = \mathbf{V}\mathbf{C} + \mathbf{w}$. For $0 \leq j < \gamma$,

$$\mathbf{Y} \cdot \frac{(\mathbf{d}_j + \mathbf{d}_{j+\gamma})}{\Phi_1}$$

$$= \mathbf{V}\mathbf{C} \cdot \frac{(\mathbf{d}_j + \mathbf{d}_{j+\gamma})}{\Phi_1} + \frac{\mathbf{w}(\mathbf{d}_j + \mathbf{d}_{j+\gamma})}{\Phi_1} \tag{54}$$

$$= \mathbf{V} \cdot [\tilde{\mathbf{C}}_1^T \quad \tilde{\mathbf{C}}_2^T \quad \cdots \quad \tilde{\mathbf{C}}_{2N}^T \quad \mathbf{1}_{\nu L \times 1}]^T \cdot \frac{(\mathbf{d}_j + \mathbf{d}_{j+\gamma})}{\Phi_1} +$$
$$\frac{\mathbf{w}(\mathbf{d}_j + \mathbf{d}_{j+\gamma})}{\Phi_1} \tag{55}$$

$$= \mathbf{V} \cdot [\mathbf{e}_j^T \quad \mathbf{e}_j^T \quad \mathbf{0}_{\Gamma(3) \times 1}^T \quad \cdots \quad \mathbf{0}_{\Gamma(2N) \times 1}^T \quad 0]^T \frac{1}{\Phi_1} +$$
$$\frac{\mathbf{w}(\mathbf{d}_j + \mathbf{d}_{j+\gamma})}{\Phi_1} \tag{56}$$

$$= \frac{\tilde{\mathbf{V}}_1 \cdot [\mathbf{e}_j^T \quad \mathbf{e}_j^T]^T}{\Phi_1} + \frac{\mathbf{w}(\mathbf{d}_j + \mathbf{d}_{j+\gamma})}{\Phi_1} \tag{57}$$

$$= \frac{\Phi_1 h_1}{\Phi_1} + \frac{\mathbf{w}(\mathbf{d}_j + \mathbf{d}_{j+\gamma})}{\Phi_1} \tag{58}$$

$$= h_1 + \frac{\mathbf{w}(\mathbf{d}_j + \mathbf{d}_{j+\gamma})}{\Phi_1}, \tag{59}$$

where (55), (56), (57) and (58) follow from (14), Lemma 2, (49) and (53), respectively. Therefore, $(\mathbf{d}_j + \mathbf{d}_{j+\gamma})$ provides an unbiased estimate of h_i with noise variance proportional to $|\mathbf{d}_j + \mathbf{d}_{j+\gamma}|^2$. The set of estimators $(\mathbf{d}_j + \mathbf{d}_{j+\gamma})$ can be

combined according to the maximal ratio combining such that the weightings are

$$\frac{\frac{1}{|\mathbf{d}_j+\mathbf{d}_{j+\gamma}|^2}}{\sum_{i=0}^{\gamma-1}\frac{1}{|\mathbf{d}_i+\mathbf{d}_{i+\gamma}|^2}} = \left(\sum_{i=0}^{\gamma-1}\frac{|\mathbf{d}_j+\mathbf{d}_{j+\gamma}|^2}{|\mathbf{d}_i+\mathbf{d}_{i+\gamma}|^2}\right)^{-1}. \quad (60)$$

The combined estimator is equal to $\boldsymbol{\beta}'$ in (21). By multiplying the weight in (60) on both sides of (59) and then summing over all j, (47) is proved. $\square$

Theorem 4. *The channel estimation in Algorithm 4 is given by*

$$\hat{h}_1 = h_1 + \frac{\mathbf{w}\boldsymbol{\beta}}{\Phi_1}, \quad (61)$$

which has expected value equal to h_1. Its noise variance is

$$\frac{|\mathbf{w}|^2 \cdot |\boldsymbol{\beta}|^2}{\Phi_1^2}, \quad (62)$$

which is smaller if β is the MNE instead of the PIE.

Proof. Since $\boldsymbol{\beta} = \boldsymbol{\beta}^*$ or $\boldsymbol{\beta}'$, (61) follows from Theorems 2 and 3 immediately. Due to $\mathbf{w}$ has zero mean, $\mathbb{E}[\hat{h}_1] = h_1$ and the noise variance is given by (62).

To complete the proof, we just need to show that $\boldsymbol{\beta}'$ is a feasible solution of the optimization problem in (23) because $\boldsymbol{\beta}^*$ from the MNE is the optimal solution [19, P. 304]. To check $\boldsymbol{\beta}'$ satisfying the constraints in (15)–(18), we just first show that (15)–(17) are satisfied with $\boldsymbol{\beta} = (\mathbf{d}_j + \mathbf{d}_{j+\gamma})$ for $0 \le j < \gamma$. Due to Lemma 2, (15) and (16) immediately follows and

$$(\tilde{\mathbf{C}}_1 - \tilde{\mathbf{C}}_2) \cdot (\mathbf{d}_j + \mathbf{d}_{j+\gamma}) = \tilde{\mathbf{C}}_1\mathbf{d}_j - \tilde{\mathbf{C}}_2\mathbf{d}_{j+\gamma} \quad (63)$$
$$= \mathbf{e}_j - \mathbf{e}_j \quad (64)$$
$$= 0. \quad (65)$$

Therefore, (17) is verified.

Consider $\boldsymbol{\beta} = \boldsymbol{\beta}'$. Since $\boldsymbol{\beta}'$ is a linear combination of $(\mathbf{d}_j + \mathbf{d}_{j+\gamma})$, (15)–(17) are satisfied. Finally, (18) is verified by

$$\mathbf{1}_{1\times\gamma} \cdot \tilde{\mathbf{C}}_2 \cdot \boldsymbol{\beta}' \quad (66)$$

$$= \mathbf{1}_{1\times\gamma} \cdot \tilde{\mathbf{C}}_2 \cdot \sum_{j=0}^{\gamma-1} \left(\sum_{i=0}^{\gamma-1}\frac{|\mathbf{d}_j+\mathbf{d}_{j+\gamma}|^2}{|\mathbf{d}_i+\mathbf{d}_{i+\gamma}|^2}\right)^{-1} (\mathbf{d}_j + \mathbf{d}_{j+\gamma}) \quad (67)$$

$$= \mathbf{1}_{1\times\gamma} \cdot \sum_{j=0}^{\gamma-1} \left(\sum_{i=0}^{\gamma-1}\frac{|\mathbf{d}_j+\mathbf{d}_{j+\gamma}|^2}{|\mathbf{d}_i+\mathbf{d}_{i+\gamma}|^2}\right)^{-1} \mathbf{e}_j \quad (68)$$

$$= \sum_{j=0}^{\gamma-1} \left(\sum_{i=0}^{\gamma-1}\frac{|\mathbf{d}_j+\mathbf{d}_{j+\gamma}|^2}{|\mathbf{d}_i+\mathbf{d}_{i+\gamma}|^2}\right)^{-1} \quad (69)$$

$$= 1, \quad (70)$$

where (67) follows from (21). Due to Lemma 2, (68) and (69) are obtained. By substituting (60) into (69), (70) is shown. Therefore, (15)–(17) are satisfied with $\boldsymbol{\beta} = \boldsymbol{\beta}'$ so that $|\boldsymbol{\beta}^*|^2 \le |\boldsymbol{\beta}'|^2$. The theorem is proved. $\square$

Since $\boldsymbol{\beta}$ is a function of $\mathbf{C}$ which is independent of M, the noise variance in (62) is independent of M. When Φ_1 is large, (62) approaches 0 and $\hat{h}_1$ tends to h_1 in (61).

MNE and PIE ares two approaches to construct ZF estimators and Theorem 4 show that MNE always achieves a smaller noise variance compared with PIE. Although the following example shows a special case that the difference between their noise variances is large, simulation results in Section V-B will illustrate that they usually achieve a similar amount of noise variance.

Example. *Consider $N = 2$, $L = 11$, $\nu = 2$, $\sigma_w^2 = 1$, $\eta_1 = 5$ and $\eta_2 = 2$. So, $\mathbf{c}_j$ is obtained from (3) and then $\tilde{\mathbf{C}}_j$ in (12) and $\mathbf{C}$ in (14) can be found. The noise variances for estimating h_1 are 0.2099 and 0.2379 for MNE and PIE, respectively. The MNE estimator obtained from Algorithm 2 can be written as $\boldsymbol{\beta}_1^* = -0.0749(\mathbf{d}_1 + \mathbf{d}_4) + 0.4943(\mathbf{d}_2 + \mathbf{d}_5) + 0.5806(\mathbf{d}_3 + \mathbf{d}_6)$, where $\mathbf{d}_i$ is defined in Algorithm 3. It is interesting to see that MNE provides a better linear combination of $(\mathbf{d}_i + \mathbf{d}_{i+\gamma})$ by allowing negative coefficients in contrast to how the coefficients are chosen in PIE according to (60).*

C. Estimation of Data

Theorem 5. *In Algorithm 4, the estimated symbol $\hat{b}_1[k]$ in (26) is given by*

$$\frac{h_1 b_1[k]}{\hat{h}_1} + \frac{(M-1)\mathbf{w}\cdot\boldsymbol{\alpha}}{2\Phi_1\hat{h}_1} \quad (71)$$

for some k. It is a ZF estimation of $b_1[k]$.

Proof. Consider

$$\frac{M-1}{2\Phi_1\hat{h}_1}\mathbf{Y}\boldsymbol{\alpha}$$

$$= \sum_{i=1}^{N} \left(\frac{\Phi_i h_i}{M-1}(\mathbf{V}_i\tilde{\mathbf{C}}_{2i-1} + (M-1-\mathbf{V}_i)\tilde{\mathbf{C}}_{2i}) \cdot \frac{(M-1)\boldsymbol{\alpha}}{2\Phi_1\hat{h}_1}\right)$$
$$+ \frac{\Phi_0 \mathbf{1}_{1\times\nu L}\cdot(M-1)\boldsymbol{\alpha}}{2\Phi_1\hat{h}_1} + \frac{\mathbf{w}\cdot(M-1)\boldsymbol{\alpha}}{2\Phi_1\hat{h}_1} \quad (72)$$

$$= \sum_{i=1}^{N} \left(\mathbf{V}_i\tilde{\mathbf{C}}_{2i-1} + (M-1-\mathbf{V}_i)\tilde{\mathbf{C}}_{2i}\right) \cdot \frac{h_1\boldsymbol{\alpha}}{2\hat{h}_1}$$
$$+ \frac{(M-1)\mathbf{w}\cdot\boldsymbol{\alpha}}{2\Phi_1\hat{h}_1} \quad (73)$$

$$= \left(\mathbf{V}_1\tilde{\mathbf{C}}_1 + (M-1-\mathbf{V}_1)\tilde{\mathbf{C}}_2\right) \cdot \frac{h_1\boldsymbol{\alpha}}{2\hat{h}_1} + \frac{(M-1)\mathbf{w}\cdot\boldsymbol{\alpha}}{2\Phi_1\hat{h}_1} \quad (74)$$

$$= (b_1[k] - (M-1-b_1[k]))\frac{h_1}{2\hat{h}_1} + \frac{(M-1)\mathbf{w}\cdot\boldsymbol{\alpha}}{2\Phi_1\hat{h}_1} \quad (75)$$

$$= \frac{h_1 b_1[k]}{\hat{h}_1} - \frac{M-1}{2} + \frac{(M-1)\mathbf{w}\cdot\boldsymbol{\alpha}}{2\Phi_1\hat{h}_1}, \quad (76)$$

where (72) and (73) follow from (13) and (39), respectively. Due to (40), (74)–(75) follow, where $b_1[k]$ is used to denote the $\lfloor\frac{\gamma}{2}\rfloor$-th element in $\mathbf{V}_1$. By substituting (76) into (26), (71) is obtained. A ZF estimation is obtained from (71) because $\hat{h}_1$ is obtained from a ZF estimator and $\boldsymbol{\alpha}$ is a function of $\mathbf{C}$ which is independent of b_j and h_j for $j > 1$.

$\square$

From Theorem 5, the additive noise variance in (71) is proportional to $(M-1)^2$. When Φ_1 is large, the last term

in (71) vanishes and h_1 tends to $\hat{h}_1$ from (61) so that $\hat{b}_1[k]$ approaches to $b_1[k]$.

D. Zero-Forcing Estimator

We have explained why MNE and PIE can be seen as ZF estimators for the channel gains. Theorem 5 shows that the estimator for the data is also a ZF estimator. It is interesting to know if Minimum Mean Square Error (MMSE) estimator may offer any benefit. Since direct line-of sight between transmitter and receiver is often assumed in visible light communications and positioning, interference power is typically much larger than the noise power. An example in [22, Section VII-B] with parameters chosen from experimental results shows that the difference between ZF estimator and MMSE estimator is insignificant. Therefore, in this paper we will focus on estimators which are built on ZF and do not require prior knowledge of the signal-to-noise ratio value.

E. Complexity Analysis

We now show that MNE has a larger computational cost when compared with PIE. Consider the matrix $\mathbf{A}$ in Algorithm 2 for MNE. Since $\omega \geq 0$ and $\nu \geq 2$,

$$
\begin{aligned}
&(2N-1)(\nu+1) - \omega + 2 \\
&\leq (2N-1)\nu + 2N + 1 \\
&< 2N\nu + 2N\nu \\
&< \nu L,
\end{aligned}
\tag{77}
$$

where the last inequality follows from Definition 1. By applying the singular value decomposition algorithm to compute $\mathbf{A}^\dagger$, the major computational cost in Algorithm 2 is given by $\mathcal{O}((\nu L)^2((2N-1)(\nu+1) - \omega + 2)) = \mathcal{O}(\nu^3 L^2 N)$ from applying [23, Fig. 8.6.1] with $m = \nu L$ and $n = (2N-1)(\nu+1) - \omega + 2$, where $m \geq n$ due to (77).

To calculate the computational cost of PIE estimator, we only need to consider the complexity to compute (21) from a given $\mathbf{C}^\dagger$, because $\mathbf{C}^\dagger$ is required in Algorithm 4 regardless of the choice of channel estimator. From Steps 4 and 5 in Algorithm 1, $\tilde{\mathbf{C}}_1$ has $\gamma \leq \nu + 1$ rows in $\mathbf{C}$. Together with $\mathbf{d}_j$ being a column vector with length νL, the total number of summations and multiplications in (21) has computational cost given by $\mathcal{O}(2\nu^2 L + 2\nu^2 + 4\nu L + 3\nu - 1) = \mathcal{O}(\nu^2 L)$, which is much smaller than that of MNE.

The major computational cost in Algorithm 1 comes from calculating $\mathbf{C}^\dagger$, which is given by $\mathcal{O}((\nu L)^2(2N(\nu+1) - \omega + 1)) = \mathcal{O}(\nu^3 L^2 N)$. Step 1 in Algorithm 1 requires FL-point DFT for L rows that has complexity $\mathcal{O}(L \cdot (FL \log_2(FL)))$ [24]. From the simulation results in Section V, it is reasonable to consider $F \approx \nu$ so that the complexity of Step 1 is thus given by $\mathcal{O}(\nu L^2 \log_2(\nu L))$. Hence, the total complexity of Algorithm 1 is given by $\mathcal{O}(\nu^3 L^2 N)$. Notice that the computational complexity of Algorithm 4 is given by $\mathcal{O}(\nu L)$, which is mainly due to the evaluation of (25) and (26).

F. Rates and Latency

Both channel estimation rate and symbol rate are $\frac{1}{T_c L}$ because new estimates are generated after waiting a duration

TABLE II: Transmitters and receiver simulation parameters

Transmitters configuration	Values
LED half power-angle $\phi_{1/2}$	$\frac{\pi}{3}$ rad
Background light intensity Φ_0	0.196 μA
Codeword length L	17 (unless otherwise specified)
Receiver configuration	**Values**
Number of PD	1
PD's Lambertian parameter	1.4
PD's FOV	$\frac{\pi}{2}$ rad
PD's responsivity R_p	22 nA/lux
Receiver's area A	15 mm^2
σ_{noise}^2	$2.0856 \times 10^{-6} + 4.8613 \times \frac{R_p(\sum_{i=1}^N P_i + \Phi_0)}{A} [V^2]$ [5]

of $T_c L$ for updating $\mathbf{Y}$ in Step 6 in Algorithm 4. Since the middle columns of $\tilde{\mathbf{C}}_1$ and $\tilde{\mathbf{C}}_2$ are used to construct $\boldsymbol{\alpha}$ in Step 3, the message conveyed by the middle element in $\mathbf{Y}$ is estimated. The latency of the system is therefore considered as the time difference between the middle and the last elements in $\mathbf{Y}$ being transmitted. This is equal to $\frac{\nu T_C L}{2}$.

G. System Design

It is possible to use other schemes such as [1] to simultaneously estimate the channel gains and message symbols. However, the scheme in [1] relies on receiving a lot of message symbols which are generated from a uniform distribution so that the average power of these symbols can be used to estimate channel gains. This is why only one codeword is used to construct the transmit signal in [1, Eqn. (5)]. In this paper, we propose a new transmitter design together with the MNE and PIE estimators, which does not require a lot of received symbols because the estimators acting on $\mathbf{Y}$ can cancel out the randomness coming from the message symbols in $\mathbf{V}_i$. This important property has been used in (42)–(46) and the proofs of Theorems 2 and 4. Most importantly, this property enables our system to simultaneously estimate channel gains and message symbols at the rate of $\frac{1}{T_c L}$ as explained in the remarks under Algorithm 4.

One of the key differences between our system and OFDMA systems for VLC is explained here. Our scheme can be interpreted as follows. Each of the N transmitters independently generates cosine waves with DC-offsets and then the waves are amplified according to its source messages. Since the transmitters are asynchronous, the time lags among them are arbitrary so that the cosine waves may start and change their amplitudes according to the messages *at different time* (cf. the model in Fig. 3). Sampling of the superposition of the cosine waves is processed by a receiver.

V. SIMULATION RESULTS

In this section, we first provide simulation results for the error probability of time lag η_i estimation, before we compare MNE and PIE and show their resulting channel gain estimation errors. We will then show the performance of the proposed multiple access scheme Sine-MA in comparison with the state-of-the-art asynchronous multiple access schemes in the literature in terms of the BER of decoded data and their system throughput.
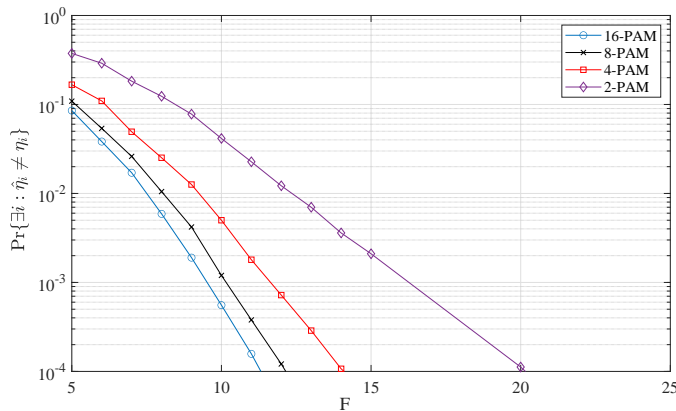
Fig. 4: The probability that the estimate $\hat{\eta}_i$ and the true η_i are different for any LED i is plotted against F for $\Phi_i = 1000$ lm and $N = 4$.

Fig. 5: The MSE of channel gain ratio versus ν for 32-PAM, $N = 4$ and $\Phi = 1000$ lm.

We assume that all transmitters have the same average optical flux Φ_i and η_i is an integer randomly generated from $[0, L-1]$ with a uniform distribution in each simulation. Fair bits are generated as data and encoded by Gray-coded M-PAM (Pulse-Amplitude Modulation) to define $b_i[k]$. The parameters of the transmitters and receiver configuration are listed in Table II.

A. Estimation of time lag η_i

Assume that 4 LEDs are installed and their (x, y, z) coordinates in meters are $(1, 1, 3)$, $(1, 2, 3)$, $(2, 1, 3)$ and $(2, 2, 3)$, and the coordinates of the receiver are $(1.5, 1.5, 1)$. The average transmitting optical flux per chip Φ_i is set to 1000 lm.

In Fig. 4, the probability that the set $\{\hat{\eta}_i\}$ is not equal to the set of true time lags $\{\eta_i\}$ is plotted against F for different M-PAM. The estimate $\hat{\eta}_i$ is obtained from Definition 2. The probability of error decreases with increasing F, as expected in Theorem 1. Also, the variance of b_i is equal to $\frac{M+1}{3(M-1)}$, which reduces when increasing the modulation order M. Therefore, the error probability of η_i estimation decreases with increasing modulation order M, as shown by Fig. 4.

Fig. 4 reveals that the probability of error of η_i estimation is less than 10^{-4} for $F > 20$ and decays exponentially fast. Note that it is possible to achieve a transmission rate higher than 10^6 symbols per second in VLC [25]. If the receiver's displacement and the change in the background light intensity are negligible within 10^{-2} seconds, h_i and Φ_0 can be seen as invariant for more than 10^4 symbols. For example, if $L = 17$, F can be selected up to $\left\lfloor \frac{10^4}{L} \right\rfloor = \left\lfloor \frac{10^4}{17} \right\rfloor = 588$. Therefore, we assume that $\hat{\eta}_i = \eta_i$ for all i in the following simulations.

B. MNE versus PIE in channel estimation

Using the same set of LED locations and Φ_i, we investigate the channel gain estimation error while comparing the performance of MNE and PIE. Since the estimated channel gain appears in the denominator in (26) and Theorem 5, it is more meaningful to consider the ratio instead of the difference
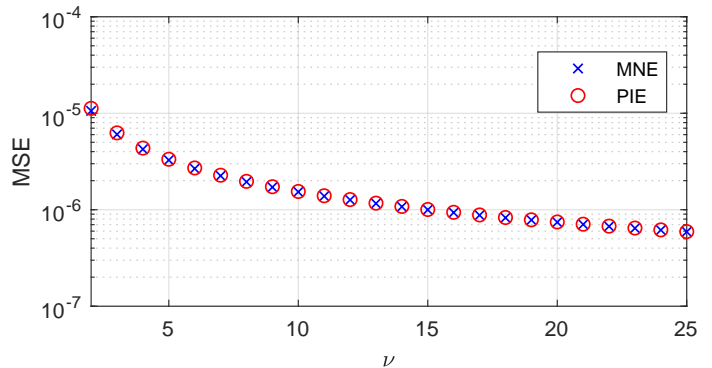
between the estimated and the true channel gains. The mean square error (MSE) of the channel gain ratio is defined as:

$$\text{MSE} = \frac{1}{N} \sum_{i=1}^{N} \left| 1 - \frac{\hat{h}_i}{h_i} \right|^2 = \frac{1}{N} \sum_{i=1}^{N} \left| \frac{h_i - \hat{h}_i}{h_i} \right|^2. \tag{78}$$

As shown in Fig. 5, both the MNE and PIE have MSE less than 10^{-5} for $\nu > 2$ and their MSEs decrease with increasing ν. Note that the receiver would process the signal vector $\mathbf{Y}$ of length νL, see (11), in order to estimate the channel gains. With a larger ν, more symbols are processed. This would reduce the noise impact and thus improve the MSE. The receiver complexity however would increase since $\mathbf{C}$ has a larger dimension when ν increases. The system latency $\nu L T_C$, which is shown in the remarks under Algorithm 4, also increases as ν increases. In Fig. 5, the MSE performance of MNE and that of PIE is very close. Since PIE can avoid the cost for solving the optimization problem (23) of Algorithm 2, it can be more favorable in practice.

The MSEs of MNE and PIE versus Φ_i for $\nu = 2$ and $\nu = 25$ are shown in Fig. 6. The MSEs decrease as Φ_i increases due to the reduced noise variance from Theorem 4. For transmission rate 10^6 symbols per second in VLC, if $L = 17$, the latency would be 1.7×10^{-5} seconds for $\nu = 2$ and 2.125×10^{-4} seconds for $\nu = 25$, respectively. These values are indeed very small and quite acceptable in many applications.

C. Sine-MA versus CCSE

In the following, we investigate the performance of the proposed multiple access scheme Sine-MA against CCSE [15], which is known suitable for DAS and effective for OCDMA and related [12–14].

To begin with, some technical details of CCSE are introduced. In CCSE, each LED is assigned with a base codeword of length L_b and weight w_b. Each base codeword has w_b ones. The base codeword is a random optical code [13], where the positions of ones are randomly chosen. The base codeword is extended by its cyclic shifted replica to form a codeword where the shift is different for each LED. The number of replica used for the codeword extension is denoted by E_{CCSE}. Therefore, the codeword length becomes $L_b(E_{\text{CCSE}} + 1)$ and
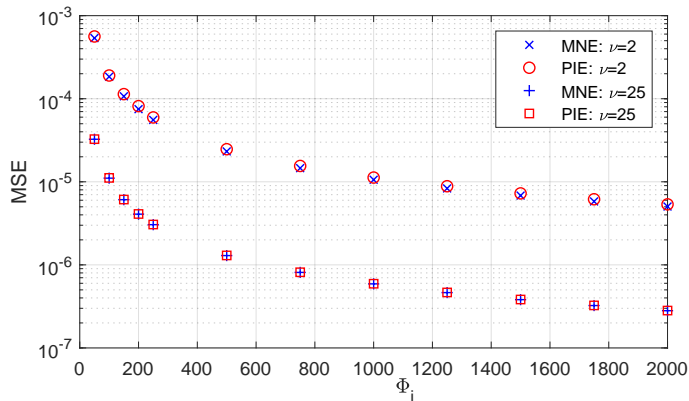
Fig. 6: The MSE of channel gain ratio versus Φ_i for 32-PAM, $N = 4$ and $\nu = 2$ and 5, respectively.

Fig. 7: The location of LEDs.

Fig. 8: System throughput versus the number of LEDs for BER less than 10^{-4}.

the weight is $w_b(E_{\text{CCSE}} + 1)$. One bit of data is transmitted by each codeword. An LED transmits the codeword or simply no signal when the data is 1 or 0, respectively. So the system throughput is given by:

$$\rho_{\text{CCSE}} = \frac{N}{L_b(E_{\text{CCSE}} + 1)}. \tag{79}$$

For data decoding, the receiver looks in the received signal for the specific $w_b(E_{\text{CCSE}} + 1)$ positions of LED i's codeword. The receiver decodes as one if pulses are detected in those positions. Otherwise, the receiver decodes as zero. The selection of E_{CCSE} is flexible but E_{CCSE} affects the trade-off between BER and system throughput. For a larger E_{CCSE}, the system throughput from (79) decreases but the BER would be reduced, as shown in [15, Eqn. (1)]. Since channel estimation is not mentioned in [15], we will consider an optimistic case that the receiver of CCSE can have perfect knowledge about the channel gains in our simulations. In this case, the constant offset and the ambient light in the received signal are perfectly estimated and eliminated. Even CCSE is considered in an optimistic case, Sine-MA will be shown to perform better.

1) System throughput versus the number of LEDs: We investigate how the system throughput is affected by the number of LEDs. The LEDs are located according to the configuration illustrated by Fig. 7, where LEDs are regularly placed over the space at a height of 3 meters and separated by a distance of 1 meter from their closest LEDs. The receiver has a single PD and is located at the height of 1 meter and in the middle of the x- and y-coordinates of the LEDs. Assume that the chip duration T_c is equal to the inverse of the modulation frequency of the LEDs so that the throughput measured in bits/chip is equivalent to the throughput measured in bits/sec/Hz. For a fair comparison, we fix the average transmitted optical flux and the maximum transmitted optical flux of both schemes to 1000 lm and 2500 lm, respectively. According to [15], the number of ones in the codewords of CCSE is much smaller than the number of zeros, e.g., the number of ones is 3 while the number of zeros is 22. Therefore, a constant offset is added to the transmitted signal of CCSE to meet the required average and maximum optical power constraints of VLC.
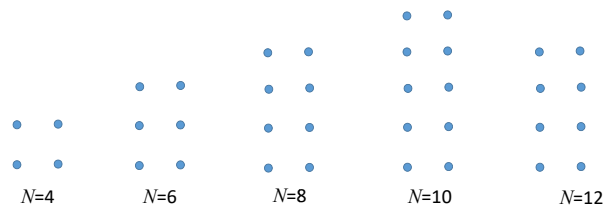
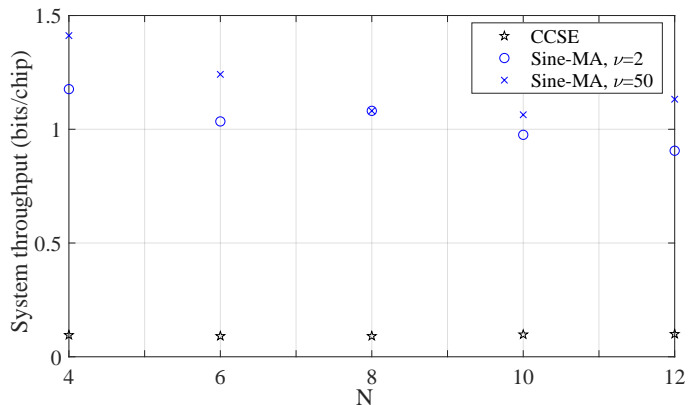In the simulations, $w_b = 3$ is selected, which is the optimum weight for the base codewords with length $L_b \leq 150$ [15]. For each N, simulations with different values of E_{CCSE} are performed and the smallest value of E_{CCSE} achieving $\text{BER}_{\text{CCSE}} \leq 10^{-4}$ is selected since it would give the largest throughput according to (79). Here, 10^{-4} is chosen because it is a common BER considered in communication systems.

The system throughput of Sine-MA is given by:

$$\rho_{\text{Sine-MA}} = \frac{N \log_2 M}{L}. \tag{80}$$

Simulations of Sine-MA for different pairs of (L, M) are performed where $M = 2^i$ for a positive integer i. Table III shows the pair of (L, M) that maximizes (80) and satisfies $\text{BER}_{\text{Sine-MA}} \leq \text{BER}_{\text{CCSE}} \leq 10^{-4}$ for each N.

The system throughput of CCSE and Sine-MA versus the number of LEDs is shown in Fig. 8. For Sine-MA, $\nu = 50$ outperforms $\nu = 2$ due to the more accurate channel estimation. The throughput of Sine-MA is at least 9 times greater than that of CCSE due to the facts: 1) The codeword length of Sine-MA is almost $4N$, while the codeword length of CCSE is at least $10N$. 2) More than one information bit per codeword can be transmitted by Sine-MA using M-PAM, e.g., 32-PAM, however only one bit per codeword can be transmitted in CCSE.

In our simulations, $L \approx 4N$ is selected and hence the system throughput of Sine-MA defined according to (80) is not sensitive to N (i.e., the number of LEDs) because

$$\rho_{\text{Sine-MA}} = \frac{N \log_2 M}{L} \approx \frac{N \log_2 M}{4N} = \frac{\log_2 M}{4}. \tag{81}$$

TABLE III: The chosen pairs of (L, M) of Sine-MA considered in Fig. 8.

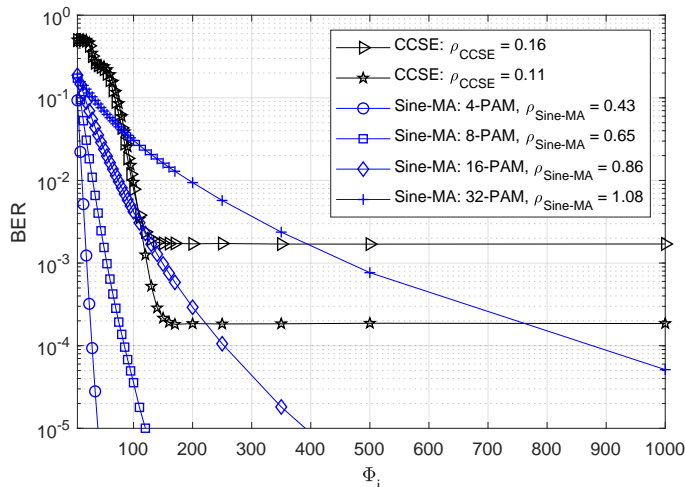| N	(L, M) **for** $\nu = 2$	(L, M) **for** $\nu = 50$
4	(17, 32)	(17, 64)
6	(29, 32)	(29, 64)
8	(37, 32)	(37, 32)
10	(41, 16)	(47, 32)
12	(53, 16)	(53, 32)

Fig. 9: BERs of Sine-MA and CCSE versus the average transmitted optical flux for $N = 8$ and $\nu = 2$. Note that the system throughput for Sine-MA is much larger than the system throughput of CCSE.

2) BER versus average transmitted optical flux: Since Sine-MA achieves much higher system throughput than CCSE as shown in Fig. 8, we compare the two schemes with the different system throughput. The BERs of Sine-MA and CCSE versus the transmitted optical flux for $N = 8$ are compared. For Sine-MA with $L = 37$, the system throughput is 0.43, 0.65, 0.86 and 1.08 for $M = 4$, 8, 16 and 32, respectively. Consider $\nu = 2$. For CCSE, consider $L_b = 25$, $w_b = 3$ and $E_{\text{CCSE}} = 1$ or 2. The codeword length equals to $L_b(E_{\text{CCSE}} + 1) = 25$ or 50. The system throughput is 0.16 and 0.11 for $E_{\text{CCSE}} = 1$ and 2, respectively. The maximum transmitted optical flux of both schemes is set as 2.5 times of the average transmitted optical flux. Under these settings, the BERs of Sine-MA and CCSE are shown in Fig. 9. The four curves of Sine-MA achieve BER less than 10^{-4} at $\Phi_i = 1000$ lm. The two curves of CCSE however cannot achieve BER less than 10^{-4} and they suffer from error floor due to the impact of MAI, which cannot be improved by increasing Φ_i. Although CCSE achieves a better BER than Sine-MA with 16-PAM and 32-PAM for some Φ_i's, the schemes have large difference in system throughput. When Sine-MA with 4-PAM is compared with CCSE, Sine-MA is better in terms of both the BER and throughput. Therefore, Sine-MA is a better scheme for a DAS.

D. Sine-MA versus the scheme in [1]

We can see that Sine-MA outperforms the scheme in [1] in terms of both the MSE and BER. From [1, Table I and (9)], $\gamma = 100$, $L = 11$ and the length of the received vector is $\alpha = (2\gamma+1)L+1 = 2212$. To obtain the results in Fig. 6, Sine-MA uses a much shorter received vector with length equal to $\nu L = 2 \times 17 = 34$ or $25 \times 17 = 425$, for $\nu = 2$ or 25, respectively. Since $\Phi_i = 500$ is used in [1, Table I], we also consider $\Phi_i = 500$ in Fig. 6 for a fair comparison. We can see that the MSE of Sine-MA at $\Phi_i = 500$ is less than 3×10^{-5} while the MSE in [1, Fig. 3] is larger than 10^{-4}. Channel gains are more accurately estimated in Sine-MA because data randomness does not affect the estimation. Note that accurate estimate of channel gains can also improve the BERs. In [1, Fig. 4], the BER is around 3×10^{-3} for throughput equal to 1.1 bits per chip. A fair comparison is to consider Sine-MA with 32-PAM in Fig. 9, which has throughput equal to $1.08 \approx 1.1$ bits per chip. When $\Phi_i = 500$, the BER is around 8×10^{-4}. Therefore, Sine-MA outperforms the scheme in [1].

VI. DISCUSSIONS

A. Characteristics of LED transmitters

LED transmitters have limited LED modulation bandwidth so that transmit signals may have amplitude distortion and signal clipping. LEDs also induce non-linearity in converting signals from electrical domain to optical domain. Although a possible use of pre-distorter can mitigate this problem, the resulting signals still suffer from some distortions. Furthermore, LED transmitters have the maximum and average power constraints due to illumination requirements. These constraints would affect the optimal design of codewords [22] and/or impose further distortions. More analysis and simulations can be done in future to study these effects in a DAS.

B. Multipath fading

In Section II, we assume that the received power mainly comes from the direct LoS path. If non-line-of-sight (NLoS) components in the received power are not negligible, indeed our scheme can be extended by appending some zeros in the transmit symbols to act as guard time. Then, $\mathbf{B}$ in Definition 2 and $\tilde{\mathbf{C}}_j$ and $\mathbf{V}_i$ in Algorithm 1 have to be modified accordingly. An alternative approach is to append cyclic prefix instead of zeros. Since this paper serves as the first step to propose a multiple access scheme for DAS, the extension for multipath components is left as future work.

VII. CONCLUSION

This paper has proposed a novel multiple access scheme Sine-MA (sinusoidal-based multiple access), which is suitable for decentralized asynchronous VLC systems. The proposed scheme reduces the system complexity and cost by avoiding the need of central unit and backbone network for coordination. It allows transmitters to start transmitting at arbitrary different times. Each transmitter is assigned two codewords with length approximately equal to four times the number of transmitters in the system. A receiver can obtain one estimate

of channel gain and one estimate of transmitted message symbol from each transmitter per the duration of receiving one codeword. Sine-MA is applicable to systems which support both visible light communications and positioning.

Since the transmitters may start to transmit at different times, they may be delayed by different time lags. We have analytically proved that in our proposed scheme, the probability of errors in the estimation of time lags vanishes as the number of received symbols grows. Simulation results have demonstrated that our scheme can support small error probability by requiring only a few hundreds of received symbols, which is a small amount and very affordable in practical systems.

Two channel gain estimators have been proposed in this paper. Based on the solution of a linear optimization problem, the proposed minimal noise variance estimator (MNE) eliminates both the multiple access interference (MAI) and ambient-light interference and minimizes the noise variance experienced at the receiver. On the other hand, the pseudo-inverse estimator (PIE) can estimate channel gains with smaller complexity and achieves a similar level of estimation error compared with MNE. Both of them are proved to be unbiased. Besides, the formulas for their noise variances have been derived.

The proposed Sine-MA also supports data transmission. When comparing Sine-MA against CCSE, simulation results have shown that Sine-MA significantly outperforms CCSE in BERs for the same system throughput. By increasing the transmit optical power, CCSE suffers from MAI which causes error floor in the BER curves but the BER of Sine-MA is strictly decreasing and clearly much more favorable.

REFERENCES

[1] A. A. Saed, S.-W. Ho, J.-M. Gorce, and C. S. Chen, "Minimal noise variance decoder for uncoordinated multiple access in VLC," in *IEEE VTC-Spring*, 2017, pp. 1–5.

[2] M. Noshad and M. Brandt-Pearce, "Application of expurgated PPM to indoor visible light communications – Part II: Access networks," *J. Lightwave Technol.*, vol. 32, no. 5, pp. 883–890, 2014.

[3] A. A. Saed, S.-W. Ho, and C. W. Sung, "Adaptive modulation for two users in VLC," in *IEEE Globecom Workshops*, 2015, pp. 1–6.

[4] M. H. Shoreh, A. Fallahpour, and J. A. Salehi, "Design concepts and performance analysis of multicarrier CDMA for indoor visible light communications," *IEEE J. Opt. Commun. Netw.*, vol. 7, no. 6, pp. 554–562, 2015.

[5] M. Yasir, S.-W. Ho, and B. N. Vellambi, "Indoor positioning system using visible light and accelerometer," *J. Lightwave Technol.*, vol. 32, no. 19, pp. 3306–3316, 2014.

[6] Y. Hou, S. Xiao, H. Zheng, and W. Hu, "Multiple access scheme based on block encoding time division multiplexing in an indoor positioning system using visible light," *IEEE J. Opt. Commun. Netw.*, vol. 7, no. 5, pp. 489–495, 2015.

[7] S. Dimitrov and H. Haas, *Principles of LED Light Communications: Towards Networked Li-Fi*. Cambridge University Press, 2015.

[8] W. Zhang, M. Chowdhury, and M. Kavehrad, "Asynchronous indoor positioning system based on visible light communications," *J. Opt. Engineering*, vol. 53, no. 4, Apr. 2014.

[9] S. De Lausnay, L. De Strycker, J. Goemaere, N. Stevens, and B. Nauwelaers, "Optical CDMA codes for an indoor localization system using VLC," in *Intl. Workshop in Optical Wireless Communications*, 2014, pp. 50–54.

[10] M. Yasir, A. A. Saed, and S.-W. Ho, "Uncoordinated multiple access scheme for VLC systems with positioning capability," in *Australian Communications Theory Workshop (AusCTW)*, 2016, pp. 118–123.

[11] S.-W. Ho and C. W. Sung, "Uncoordinated multiple access schemes for visible light communications and positioning," in *IEEE Int. Symp. on Inf. Th. (ISIT)*, 2016, pp. 350–354.

[12] M. F. Guerra-Medina, O. González, B. Rojas-Guillama, J. A. Martín-González, F. Delgado, and J. Rabadán, "Ethernet-OCDMA system for multi-user visible light communications," *Electron. Lett.*, vol. 48, pp. 227–228, 2012.

[13] J. A. Martin-Gonzalez, E. Poves, and F. J. Lopez-Hernandez, "Random optical codes used in optical networks," *IET Commun.*, vol. 3, no. 8, pp. 1392–1401, 2009.

[14] J. A. Martín-González, O. González, E. Poves, F. J. López-Hernández, and R. Pérez-Jiménez, "Code acquisition of random optical codes in optical code-division multiple-access," *IET Commun.*, vol. 6, no. 18, pp. 3176–3188, 2012.

[15] O. González, J. A. Martín-González, M. F. Guerra-Medina, F. J. López-Hernández, and F. A. Delgado-Rajó, "Cyclic code-shift extension keying for multi-user optical wireless communications," *Electron. Lett.*, vol. 51, no. 11, pp. 847–849, 2015.

[16] S. Jung, D. Kwon, S. Yang, and S. Han, "Reduction of inter-cell interference in asynchronous multi-cellular VLC by using OFDMA-based cell partitioning," in *18th Intl. Conf. on Transparent Optical Networks (ICTON)*, 2016, pp. 1–4.

[17] T. Komine and M. Nakagawa, "Fundamental analysis for visible-light communication system using LED lights," *IEEE Trans. Consumer Electron.*, vol. 50, pp. 100–107, 2004.

[18] Z. Ghassemlooy, W. Popoola, and S. Rajbhandari, *Optical Wireless Communications: System and Channel Modelling with Matlab®*. CRC Press, 2019.

[19] S. Boyd and L. Vandenberghe, *Convex Optimization*. Cambridge university press, 2004.

[20] T. M. Cover and J. A. Thomas, *Elements of Information Theory*. USA: Wiley-Interscience, 2006.

[21] T. S. Han and M. Hoshi, "Interval algorithm for random number generation," *IEEE Transactions on Information Theory*, vol. 43, no. 2, pp. 599–611, 1997.

[22] S.-W. Ho, "The interplay between block design theory and channel estimation in visible light system," *IEEE Trans. Inform. Theory*, vol. 67, no. 2, pp. 991–1007, 2021.

[23] G. H. Golub and C. F. Van Loan, *Matrix Computations*, 4th ed., ser. Johns Hopkins Studies in Mathematical Sciences. Baltimore: Johns Hopkins University Press, 2013.

[24] P. Duhamel and M. Vetterli, "Fast Fourier transforms: A tutorial review and a state of the art," *Signal Process.*, vol. 19, no. 4, p. 259–299, Apr. 1990.

[25] S. Rajagopal, R. D. Roberts, and S. Lim, "IEEE 802.15.7 visible light communication: modulation schemes and dimming support," *IEEE Commun. Mag.*, vol. 50, no. 3, pp. 72–82, 2012.